Pergamon

Journal of Structural Geology, Vol. 17, No. 5, pp. 663 to 676, 1995

0191-8141/95 $9.50+0.00

0191-8141(94)00084-0

Shear zones as a new type of palaeostress indicator

DEEPAK C. SRIVASTAVA,* RICHARD J. LISLE and SARA VANDYCKE

Laboratory for Strain Analysis, Department of Earth Sciences, University of Wales, Cardiff CF1 3YE, U.K.

(*Received* 13 *September* 1993; *accepted in revised form* 21 *July* 1994)

Abstract—This paper proposes that shear zones act as palaeostress indicators in much the same way as brittle faults. Several hundred shear zones, from both the limbs of the Variscan Langland-Mumbles anticline (South Wales), are treated using the graphical and numerical methods of fault slip analysis.

Estimated palaeostress directions derived from shear zones are characterized by greater scatter than where brittle faults are used as stress indicators. An important reason for this is the fact that on some shear zones the direction of maximum shear stress (slip lineation) is not perpendicular to the line of *S*/*C* intersection. As a consequence, the use of slip lineations produces better solutions than cases where the slip direction is inferred as a line perpendicular to the *S*/*C* intersection.

The filtering of data to reduce the scatter in the results produces insignificant improvement and is considered unnecessary.

INTRODUCTION

Palaeostress and strain analyses provide useful constraints for understanding the geodynamic evolution of the deformed tectonites (Tobisch *et al.* 1977, Letouzey 1986, Bergerat 1987, and others). A necessary requirement for the application of these analyses is the availability of suitable markers or indicators to serve as input data. Numerous types of strain markers (e.g. oolites, pebbles, fossils, boudins, syntectonic fibres and deformation twins) have already been recognized resulting in a wealth of literature on strain analyses (Ramsay & Huber 1983). On the other hand, only a limited range of tectonic structures (e.g. joints, stylolites and brittle faults) are traditionally used for palaeostress analysis (Engelder & Geiser 1980, Hancock 1985, Bénard *et al.* 1990). With the exception of Lisle (1989a) who used sheared dykes as palaeostress indicators, the advanced methods of fault slip analysis have so far only been applied to meso-faults. In many geological situations, such a restrictive approach results in a limitation of palaeostress analysis either for the reason that a sufficient number of meso-faults are not exposed or that these faults do not contain lineations revealing unambiguously the sense and direction of movement. In order to broaden the scope of fault slip analysis we have attempted to use shear zones as stress indicators.

APPROACH

To test the usefulness of shear zones as palaeostress indicators, we examined shear zones in the Eastern Gower Peninsula, near Swansea, South Wales (Fig. 1a). This area is particularly suitable for our objectives as meso-scale shear zones are developed abundantly and the structural setting is rather simple (George 1940, Roberts 1979, Hyett 1990). Here, a Lower Carboniferous sequence of carbonate rocks was folded into an anticlinal structure (the 'Langland-Mumbles anticline', Hyett 1990) during the Variscan orogeny (Fig. 1b). This fold is characterized by a large interlimb angle (110°–136°), steeply dipping axial plane and a low axial plunge (17° towards N104°, Figs. 1b & c). A series of N–S striking, oblique slip faults with predominant strike-slip component (George 1940) cuts through the Langland-Mumbles anticline as regional-scale transverse structures (Fig. 1b).

We have selected four sites (Tutt Head, Rams Tor, Pier Head and Middle Head) to test the use of shear zones as palaeostress indicators. Two of these sites (Tutt Head and Rams Tor) are located on the southern limb and the other two (Pier Head and Middle Head) fall on the northern limb of the Langland-Mumbles anticline (Fig. 1b). We describe, in brief, the geometrical characteristics of two types of shear zones, ductile shear zones and brittle-ductile shear zones, present at each of the four sites.

Ductile shear zones

Two distinct sets of ductile shear zones with typical *S*–*C* foliations (Berthé *et al.* 1979) occur commonly in these rocks (Fig. 2a). The sense of movement is 'top-to-the-north' and 'top-to-the-south' in the first and second sets, respectively. Several lines of evidence including offset of the beds and fossils (Fig. 2b), deflection of pre-existing bedding-normal stylolites, the sense of movement of hangingwalls and the occurrence of 'pop-up' structures (Fig. 2c), all suggest a dominantly thrust type of movement on both sets of shear zones. That the deformation producing shear zones had no effect on the wall rocks is amply demonstrated by the undistorted shapes of fossil corals (Fig. 2b). In this regard, these shear zones are similar to brittle faults.

The conjugate nature of the two sets of ductile shear zones is evident from the inconsistency of their cross-

*Present address: Department of Earth Sciences, University of Roorkee, Roorkee 247 667, India.

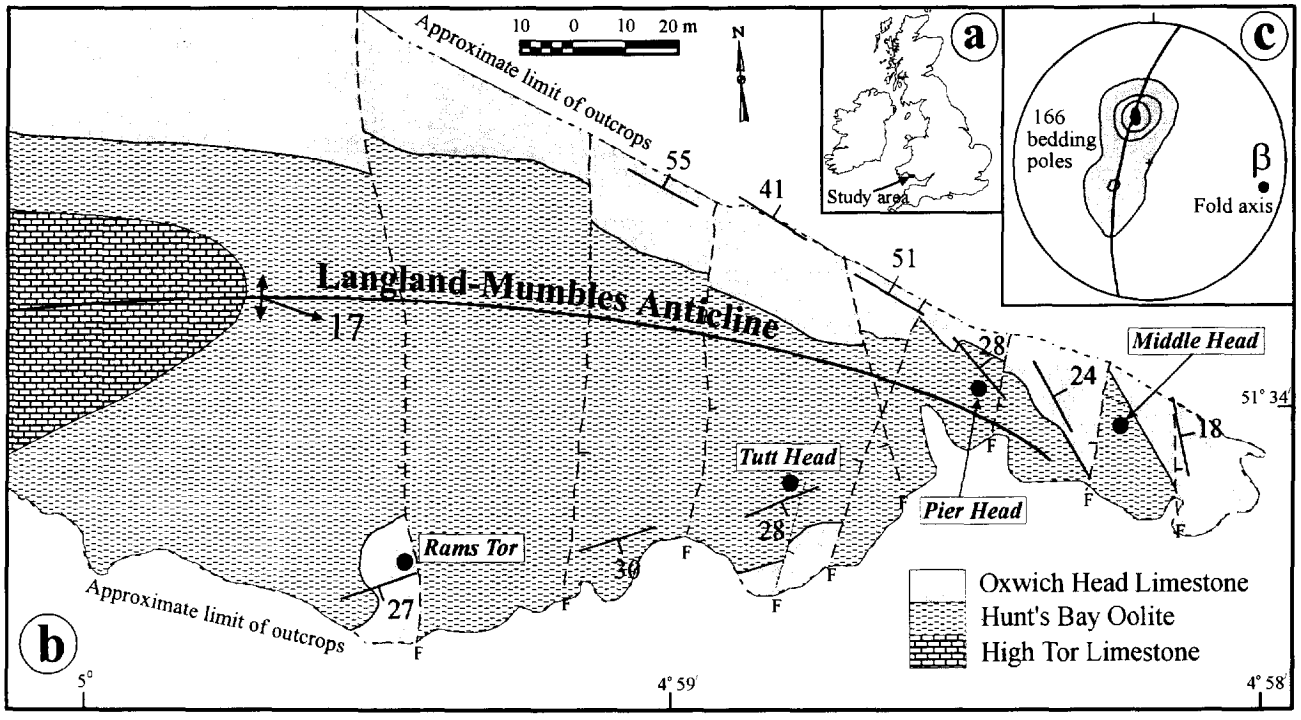

Fig. 1. (a) Location of the study area. (b) Geological and structural map of the study area (double and single headed arrows represent axial trace and axis of the Langland-Mumbles anticline, respectively. F— Fault with down throw side; formation boundaries and fault traces, after Geological Survey of Great Britain 1971). (c) Lower hemisphere, equal area projection of 166 poles to the bedding (β-fold axis of the Langland-Mumbles anticline, contours- 1–10–20–30% per 1% area).

cutting relationships, nearly equal numbers and opposite sense of displacement in the complementary sets (Fig. 2c) and the development of 'hour-glass' structures at their intersection zones (Fig. 2d). These hour-glass structures, defined by *S*-foliations are formed upon the locking-up of two shear zones belonging to complementary sets. One consequence of the development of hour-glass structures is that the same foliation is shared by both the sets within the intersection zones suggesting their conjugate nature and synchronous development (Fig. 2e).

On the basis of the nature of their internal fabric, three types of ductile shear zones can be distinguished in order of decreasing abundance, (a) shear zones consisting of closely spaced pressure solution seams (*S*-foliations; Fig. 2a), (b) those consisting of mm-thick and very closely spaced ($\leq$ 1 mm) en échelon calcite veins, and (c) those containing both the pressure solution seams and calcite veins (Fig. 2f). Despite the morphological similarities, the pressure solution seams defining *S*-foliations in the shear zones are younger than the bedding-normal stylolites. The latter are often deflected as pre-existing markers across the shear zones. Intense foliation located asymmetrically at the shear zone tips reflect high strains associated with the decay of relative displacement at the terminations of shear zones (Fig. 3a; Ramsay & Allison 1979).

Brittle-ductile shear zones

Brittle-ductile shear zones defined by the boundaries of cm–m scale en échelon calcite veins occur as conjugate pairs of dextral and sinistral sets (Fig. 3b). These two sets classify as type-I conjugate pairs of Beach (1975) on the basis of the fact that the boundary of shear zones of one set is parallel to the veins within the complementary set (Fig. 3b). In the Langland-Mumbles area, the brittle-ductile shear zones differ from the ductile shear zones in the following respects. Firstly, the brittle-ductile shear zones show both dextral and sinistral types of strike-slip motion, whereas the ductile shear zones show thrust type of movement. Secondly, most brittle-ductile shear zones contain en échelon veins whereas the ductile shear zones consist mostly of pressure solution seams. Finally and most significantly, on all the outcrops where the two types of shear zones occur together, the brittle-ductile shear zones always cut through the ductile shear zones. From these lines of field evidence, we conclude that the brittle-ductile shear zones are younger than the ductile shear zones in the Langland-Mumbles area. Thus the geometry and cross-cutting relationships suggest two shearing events arising from different stress states that can be determined by treating the ductile shear zones and brittle-ductile shear zones separately.

ASSUMPTIONS

Despite the fact that we have assumed that the shear zones behave like brittle faults for the purpose of palaeostress analysis there is a basic difference between these two types of structures. Faults develop in the elastic field whereas shear zones develop in the brittle-

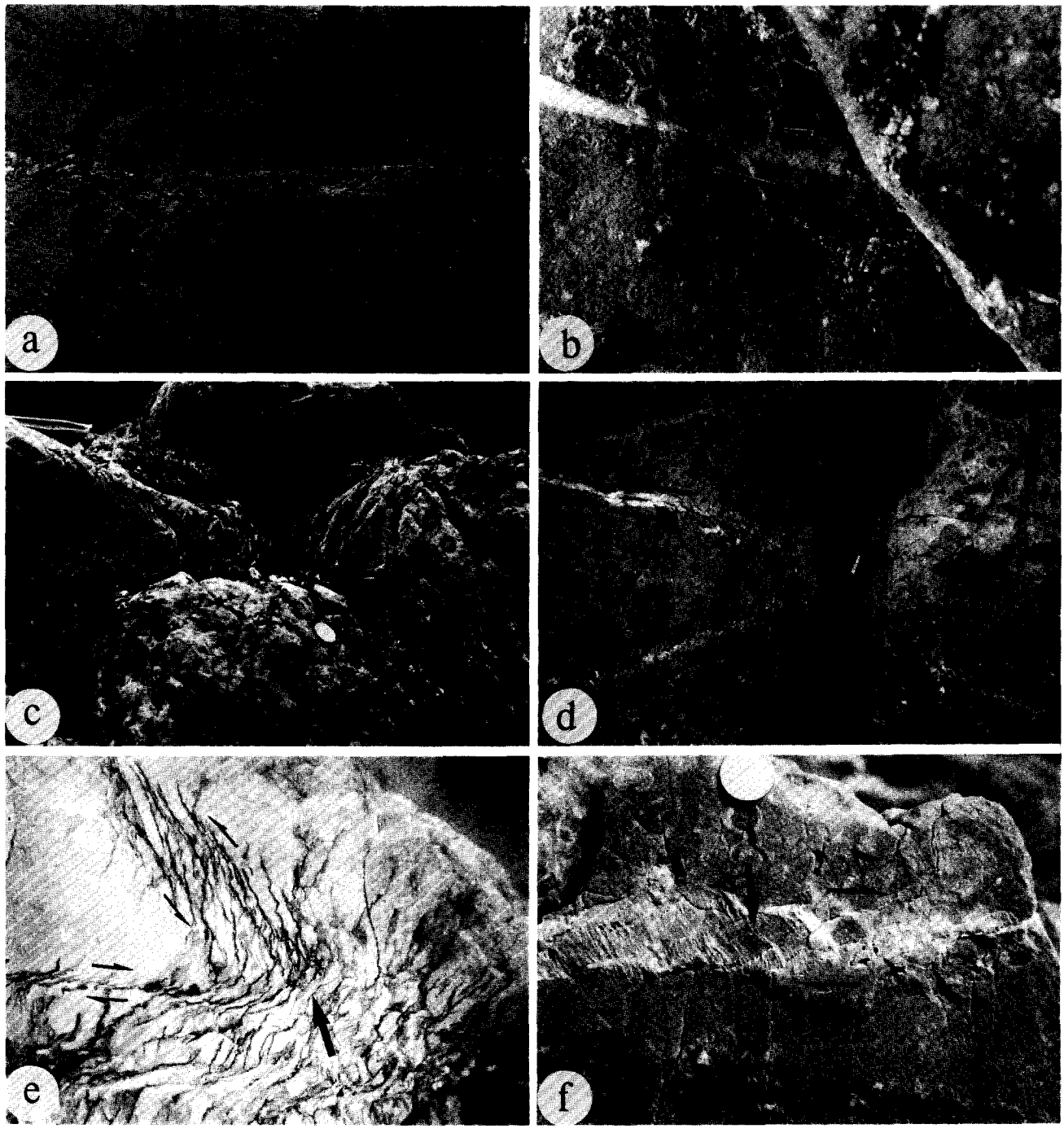

Fig. 2. (a) A typical 'top-to-the-south' ductile shear zone (N020°/35°E) showing well developed *S–C* fabric (length of shear zone 1.5 m). (b) 'Top-to-the-north' ductile shear zone (N012°/25°E) offsetting a coral. Note the undeformed shape of the coral (diameter of fossil 2 cm). (c) A conjugate pair of the ductile shear zones showing pop-up structure formed due to thrust type of movement on both the sets [the orientations of 'top-to-the-north' (sinistral) and 'top-to-the-south' (dextral) shear zones are N107°/45°S and N023°/31°E, respectively. Diameter of coin 2.4 cm]. (d) An hour-glass structure formed due to the locking up of the complementary sets of a ductile shear zone [the orientations of 'top-to-the-north' (sinistral) and 'top-to-the-south' (dextral) shear zones are N073°/45°S and N002°/30°E, respectively. Diameter of lens cover 5.5 cm]. (e) Hour-glass structure with an area (indicated by arrow) of foliation which is shared by both shear zones [the orientations of 'top-to-the-north' (sinistral) and 'top-to-the-south' (dextral) shear zones are N110°/50°S and N347°/31°E, respectively, diameter of coin 2.4 cm]. (f) En échelon calcite veins and orthogonally oriented, widely spaced pressure solution seams (indicated by arrow) defining the internal fabric within a 'top-to-the-north' ductile shear zone oriented N005°/27°S. (Diameter of coin 2.4 cm.) Location (a) and (c)–(f) Tutt Head; (b) Middle Head.

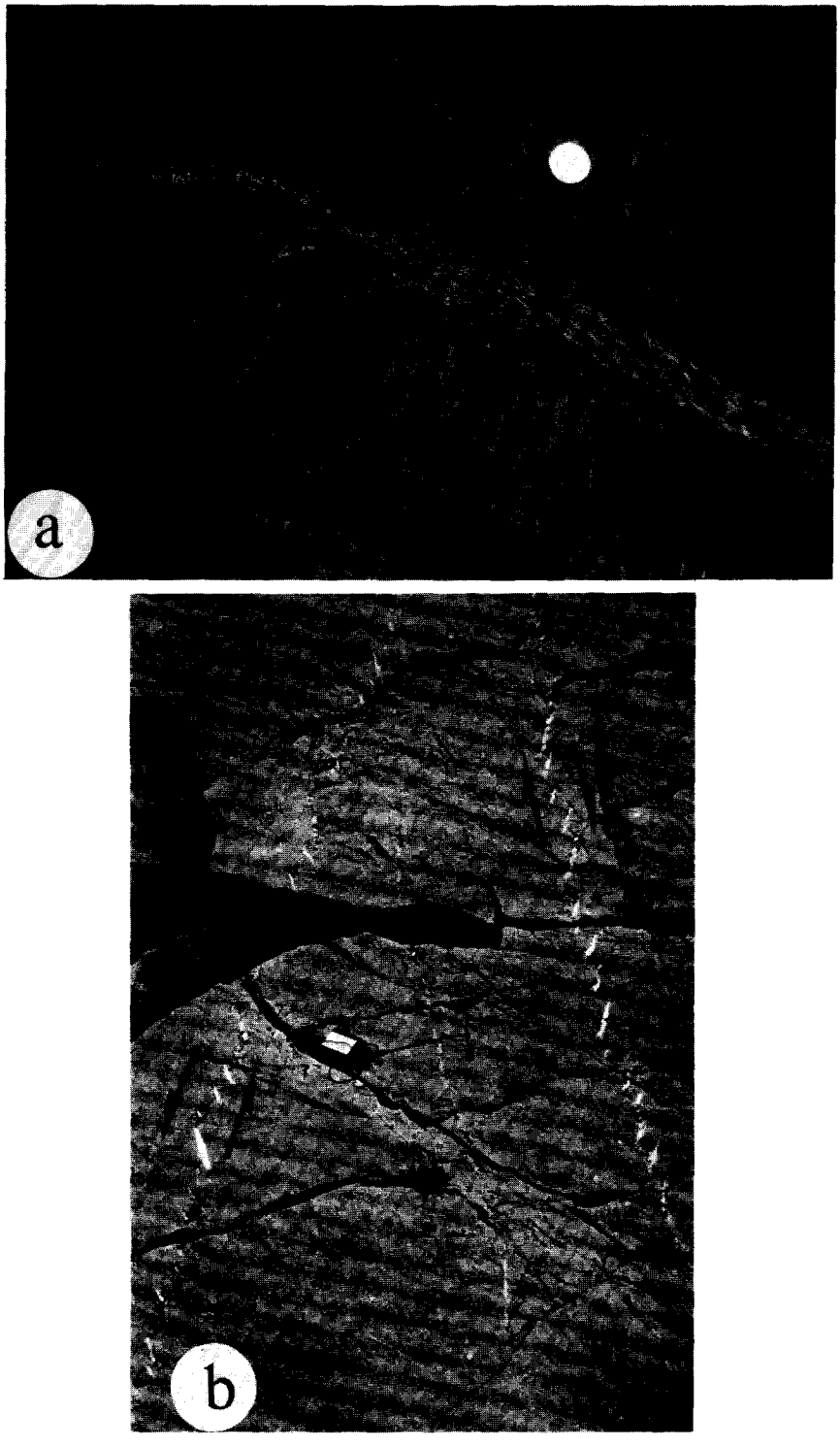

Fig. 3. (a) Intense foliations in the shortening sector around the tip of a 'top-to-the-north' ductile shear zone oriented N088°/30°S (diameter of coin 2.4 cm). (b) Beach type-I conjugate pair of brittle-ductile shear zones. The boundary of each set is parallel to the veins in the complementary set (the orientation of the dextral and sinistral sets are N172°/72°W and N204°/70°W, respectively, length of compass 9 cm). Location for (a) & (b) Tutt Head.

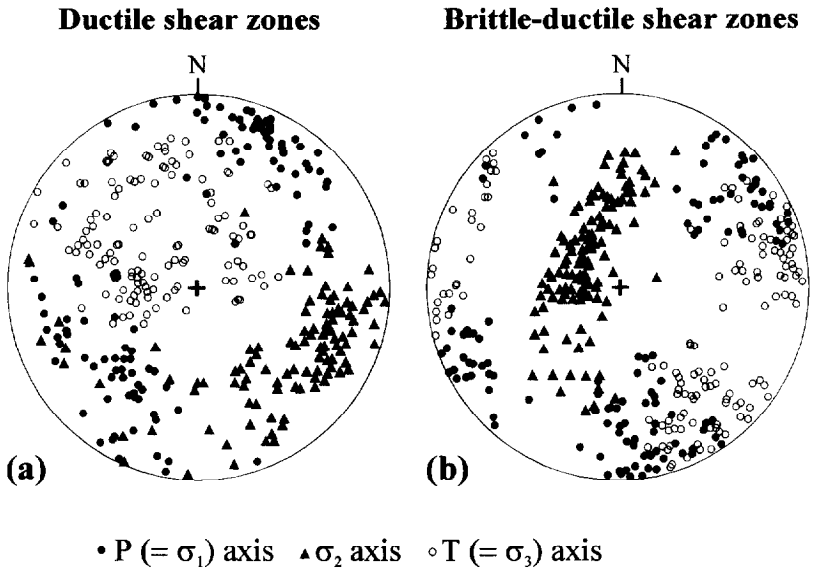

Fig. 4. An example of results from the *P–T* axes method (lower hemisphere, equal area projections). The intermediate stress axes (σ_2 shown as triangles) are determined by finding the poles to σ_1-σ_3 planes. (a) One hundred and eleven ductile shear zones from Tutt Head. (b) One hundred and twenty-five brittle-ductile shear zones from Tutt Head.

ductile or ductile regime and have a relatively long deformation history. In our examples, the shear zones are developed only on mm–m scale and are widely spaced so they contribute little to the regional structural geometry of the area.

The methodology of fault-slip analysis requires (a) slip on all the shear zones in response to a single, homogeneous state of stress, and (b) parallelism between the slip lineation and the direction of maximum resolved shear stress on each shear zone. Commonly, the nature of exposure is such that the *C*-surface of the shear zone is not available for the direct measurement of the slip lineation. To solve this problem, we have measured the orientation of internal fabric *viz.*, *S*-foliation in ductile shear zones and veins in brittle-ductile shear zones. The slip direction on the *C*-surface is assumed to be the line which is perpendicular to the line of intersection of the shear zone (*C*-surface) and the internal fabric. This assumption of the slip direction being perpendicular to the *S*/*C* intersection has been tested independently by directly measuring slip lineation in a few cases and comparing their orientations with the inferred slip directions.

One distinct advantage of using shear zones is the obvious sense of movement for every shear zone; slip sense on faults is frequently ambiguous. The slip sense is indicated unambiguously by the angular relationships between the internal fabric (*S*-foliation or vein) and the shear zone boundary (*C*-surface; Simpson & Schmid 1983).

METHODS

Several techniques for palaeostress analysis have been devised and modified during the last couple of decades (McKenzie 1969, Etchecopar *et al.* 1981, Gephart & Forsyth 1984, Michael 1984, Aleksandrowski 1985, Lisle 1987, Angelier 1990, Marrett & Allmendinger 1990). All the methods aim at inverting the field data to find the stress tensor responsible for the observed slips on variably oriented faults, assuming that the motion on faults occur in the direction of maximum resolved shear stress. These methods allow the determination of the orientations of three principal stress axes ($\sigma_1 \geq \sigma_2 \geq \sigma_3$) and a parameter expressing the relative shape of the stress ellipsoid (**R** in Lisle 1989a and Φ in Angelier 1990).

We have analysed shear zone data by both the graphical and numerical methods applied normally to striated faults. The graphical methods include the *P–T* axes method (Stauder 1962), the right dihedra method (Pegaroro 1972, Angelier & Mechler 1977) and the right trihedra method of Lisle (1988). The numerical analysis includes the direct inversion and four-dimensional exploration methods of Angelier (1990). The graphical forms of analysis are simple and easy to visualize as stereograms showing the potential fields for principal stress directions. Once the results from graphical methods are available, the results from numerical methods serve as a check and add to the accuracy of the results. Several recent papers elaborate these methods in detail (Aleksandrowski 1985, Angelier 1990, Lisle 1992).

The *P–T* axes method, originally devised to find stresses from calcite twins (Turner 1953) is commonly applied to estimate stresses from focal planes of earthquakes (Stauder 1962). In this method, a movement plane containing the slip lineation and the pole to the shear zone is constructed. The *P* and *T* axes, best estimates of the σ_1 and σ_3 axes, respectively, are located in the movement plane at 45° and 135° from the slip lineation using the correct sense of movement. The intermediate axis (σ_2) is defined by the normal to the movement plane. In the *P–T* analysis of shear zones, the σ_2-axis happens to coincide with the line of intersection

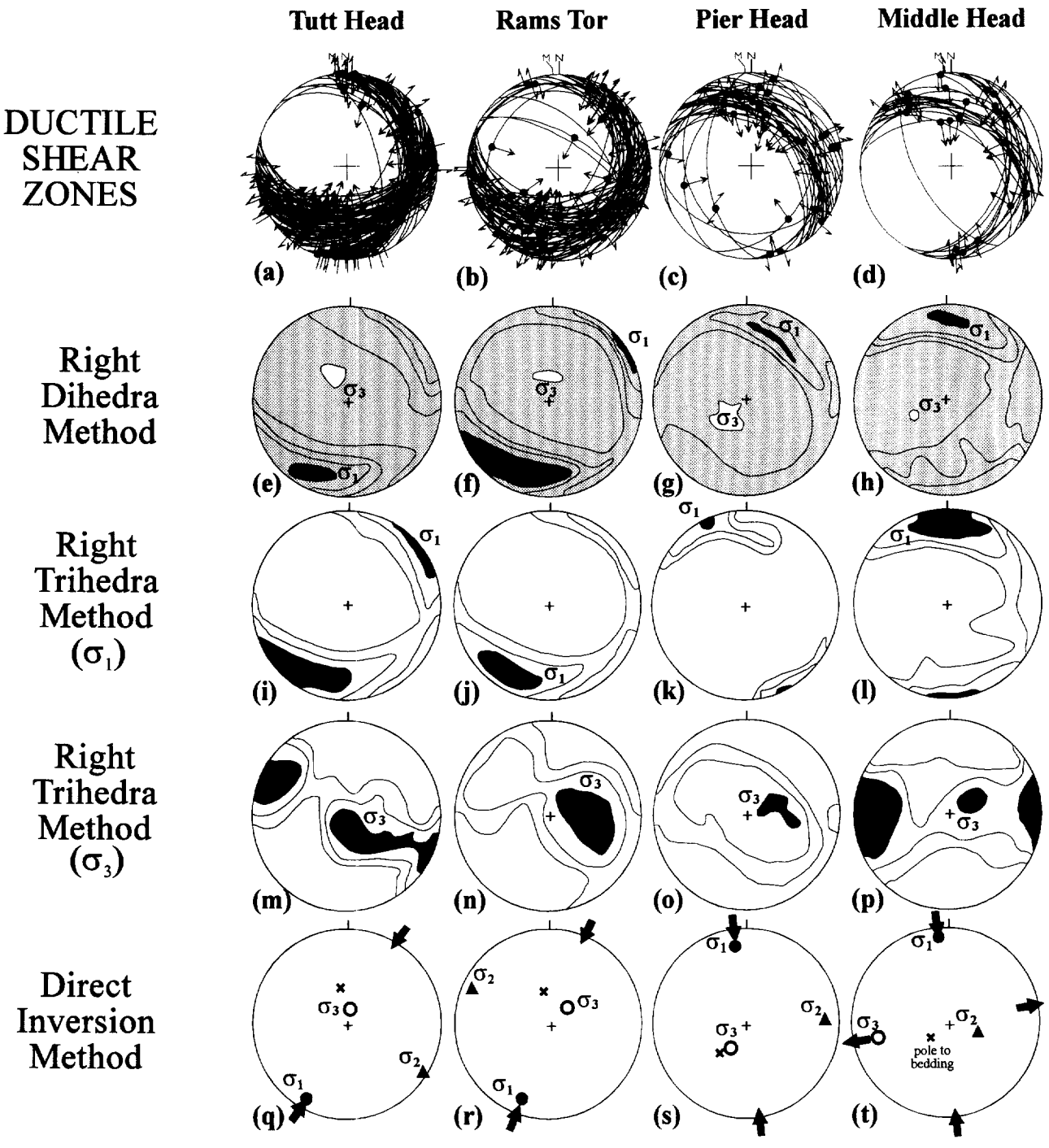

Fig. 5. Site-wise results of palaeostress analysis of ductile shear zones. (a)–(d) Ductile shear zones with slip lineations (M—magnetic north, N—geographic north). (e)–(h) Results from the dihedra method (most likely orientations of the σ_1- and σ_3-axes are shown by the maximum and the minimum contours filled in black and white, respectively). (i)–(p) Results from the trihedra method [most likely positions of the σ_1- and σ_3- axes are shown in the Figs. (i)–(l) and (m)–(p), respectively]. (q)–(t) Results from the direct inversion method (inward and outward arrows indicate the directions of the maximum compression and the maximum extension, respectively, cross indicates pole to bedding). Total number of the analysed shear zones at the sites Tutt Head, Rams Tor, Pier Head and Middle Head are 111, 91, 35 and 26, respectively; contour% per 1% area—(e) 10–50–70–80–90, (f) 10–50–60–70–80, (g) 20–60–70–80, (h) 10–50–60–70–90, (i) & (j) 30–40–50, (k) 40–45–50, (l) 30–40–50, (m) 40–45–50, and (n)–(p) 30–40–50. All lower hemisphere, equal area projections.

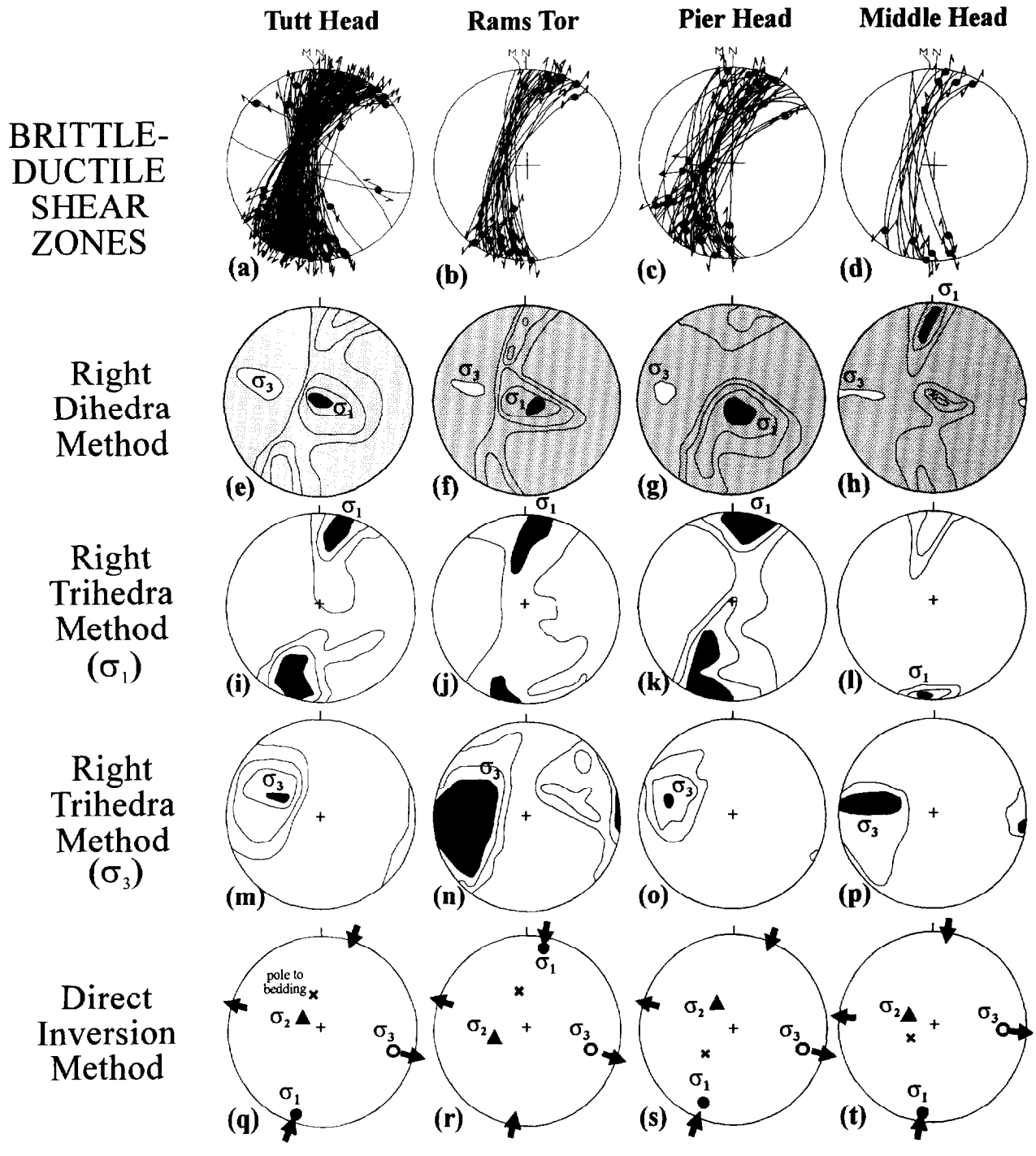

Fig. 6. Site-wise results of palaeostress analysis of the brittle-ductile shear zones. (a)–(d) Brittle-ductile shear zones with slip lineations. (e)–(h) Results from the dihedra method (most likely positions of the σ_1- and σ_3-axes are shown by the maximum and the minimum contours filled in black and white in each diagram, respectively). (i)–(p) Results from the trihedra method [most likely positions of the σ_1 and σ_3- axes are shown in the Figs. (i)–(l) and (m)–(p), respectively]. (q)–(t) Results from the direct inversion method (inward and outward arrows indicate directions of the maximum compression and the maximum extension, respectively, cross indicates pole to bedding). Total number of the analysed brittle-ductile shear zones at the sites Tutt Head, Rams Tor, Pier Head and Middle Head are 125, 27, 38 and 11, respectively; contour% per 1% area —(e)–(g) 10–60–70–80–90, (h) 1–77–88–99, (i) 30–35–40, (j) 30–40, (k) 30–35–40, (l) 50–60–70, (m) 30–40–45–50, (n) 30–35–40, (o) 40–45–50, and (p) 50–70. All lower hemisphere, equal area projections.

Table 1. Results of palaeostress analyses of ductile shear zones by the *P–T* axes method, right trihedra method and direct inversion method (DIR INV). TH—Tutt Head, RT—Rams Tor, PH—Pier Head, MH—Middle Head

		σ_1 axis (azimuth/amount)			σ_2 axis (azimuth/amount)			σ_3 axis (azimuth/amount)			Shape of the stress ellipsoid	
Site	No. of data	*P–T* axes	Tri-hedra (Lisle 1988)	Dir inv (Angelier 1990)	*P–T* axes	Tri-hedra (Lisle 1988)	Dir inv (Angelier 1990)	*P–T* axes	Tri-hedra (Lisle 1988)	Dir inv (Angelier 1990)	**R** (Lisle 1989a)	Φ (Angelier 1990)
TH	111	210/08	201/13	212/12	115/28	034/77	121/03	315/61	291/03	020/77	0.01	0.01
RT	91	208/18	209/15	202/18	295/71	310/34	296/09	356/69	102/53	052/70	0.25	0.20
PH	35	021/24	333/01	352/19	328/60	241/28	087/15	148/83	072/62	214/66	1.50	0.60
MH	26	353/03	357/13	354/09	292/64	161/76	100/60	259/53	284/08	259/28	0.09	0.08

Table 2. Results of palaeostress analyses of brittle-ductile shear zones by the *P–T* axes method, right trihedra method and direct inversion method. Abbreviations for sites same as in Table 1

		σ_1 axis (azimuth/amount)			σ_2 axis (azimuth/amount)			σ_3 axis (azimuth/amount)			Shape of the stress ellipsoid	
Site	No. of data	*P–T* axes	Tri-hedra (Lisle 1988)	Dir inv (Angelier 1990)	*P–T* axes	Tri-hedra (Lisle 1988)	Dir inv (Angelier 1990)	*P–T* axes	Tri-hedra (Lisle 1988)	Dir inv (Angelier 1990)	**R** (Lisle 1989a)	Φ (Angelier 1990)
TH	125	201/10	198/05	199/06	321/71	105/36	306/69	109/17	299/53	106/20	1.38	0.58
RT	27	169/11	202/17	010/13	295/71	096/42	257/59	076/14	289/47	107/27	0.31	0.24
PH	38	193/22	193/08	202/17	328/60	089/60	325/62	095/19	286/29	105/22	0.54	0.35
MH	11	185/08	187/11	189/07	292/64	070/67	295/65	091/25	283/20	096/24	0.61	0.38

Table 3. Measures of data dispersion indicating the degree of inhomogeneity (scatter) in the results from ductile shear zones given in Table 1. Abbreviations for sites same as in Table 1. ANG—the average angle between the observed slip direction and the direction of maximum shear stress, RUP—a function of the ANG and the amount of the maximum shear stress, P_{total}—percentage of the shear zones compatible with the results

Site	No. of data	RUP (Angelier 1988)	ANG (Angelier 1988)	P_{total} (σ_1) (Lisle 1990)	P_{total} (σ_3) (Lisle 1990)
TH	111	64%	36°	57.17%	57.75%
RT	91	67%	36°	59.91%	58.89%
PH	35	73%	41°	52.66%	53.47%
MH	26	71%	43°	61.44%	58.98%

Table 4. Measures of data dispersion indicating the degree of inhomogeneity (scatter) in the results from brittle-ductile shear zones given in Table 2. Abbreviations for sites same as in Table 1. ANG, RUP and P_{total}—same as in Table 3

Site	No. of data	RUP (Angelier 1988)	ANG (Angelier 1988)	P_{total} (σ_1) (Lisle 1990)	P_{total} (σ_3) (Lisle 1990)
TH	125	73%	47°	50.23%	51.56%
RT	27	83%	55°	47.79%	50.17%
PH	38	77%	51°	51.71%	51.49%
MH	11	68%	34°	70.23%	79.01%

Table 5. Comparison of results from the two methods of generating the slip direction data (example from ductile shear zones at the Tutt Head and Rams Tor sites). The degree of heterogeneity in these results is given in the Figs. 9(c)–(j) in terms of ANG, RUP and P_{total}%

		σ_1 axis (azimuth/amount)			σ_2 axis (azimuth/amount)			σ_3 axis (azimuth/amount)			Shape of the stress ellipsoid	
Method for determining slip direction	No. of data	*P–T* axes	Tri-hedra (Lisle 1988)	Dir inv (Angelier 1990)	*P–T* axes	Tri-hedra (Lisle 1988)	Dir inv (Angelier 1990)	*P–T* axes	Tri-hedra (Lisle 1988)	Dir inv (Angelier 1990)	**R** (Lisle 1989a)	Φ (Angelier 1990)
Directly measured slip lineation	22	018/02	178/08	195/01	108/10	082/39	104/18	280/80	284/49	289/72	1.32	0.57
Normal to *S/C* intersection	22	019/03	218/09	206/03	110/05	318/37	298/36	255/84	132/53	112/54	0.22	0.18

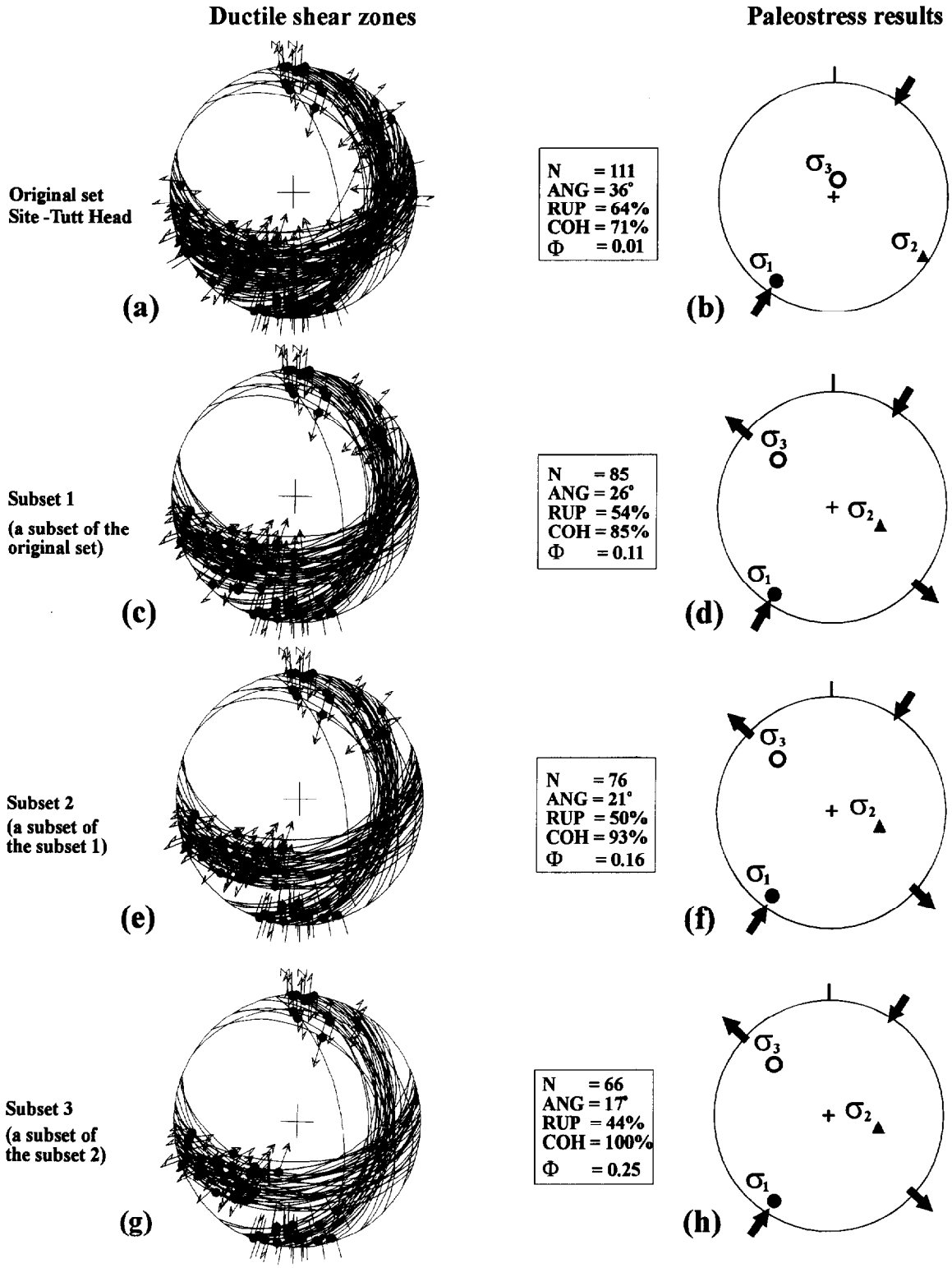

Fig. 7. Effect of dividing data (combined from Tutt Head and Rams Tor) in different subsets in order to reduce dispersion in results. The results in the Figs. (b), (d), (f) & (h) have been obtained by analysing the shear zones in the Figs. (a), (c), (e) & (g), respectively, (*N*—number of shear zones, ANG and RUP represent the dispersion in results, Φ—a parameter defining the shape of the stress tensor, COH—is the total % of the shear zones with admissible ANG and RUP values; Lower hemisphere, equal area projections; see text for details).

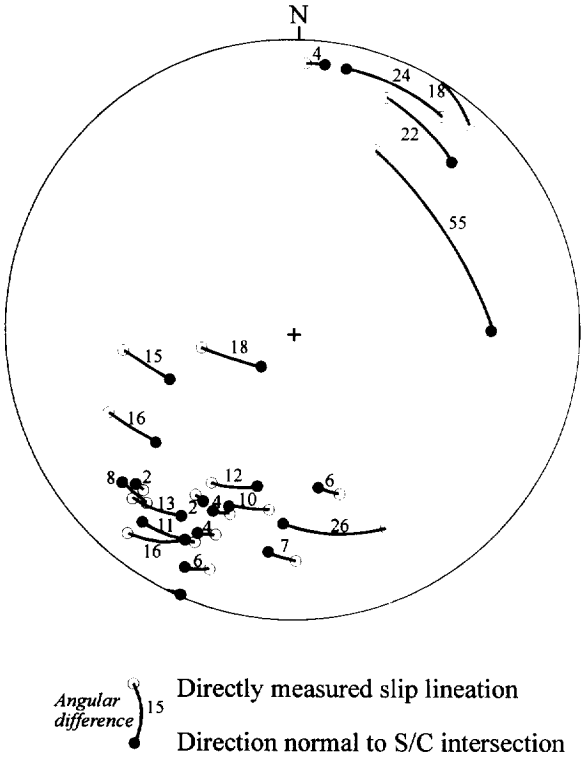

Fig. 8. Angular difference (measured in the plane of shear zone) between directly measured and reconstructed slip direction in 22 ductile shear zones combined from Tutt Head and Rams Tor sites (lower hemisphere, equal area projections).

of shear zone boundary (*C*-surface) and internal fabric (*S*-foliation or vein) as the slip direction is assumed to be 90° from the *S*/*C* intersection line. The objective of using this method is to gain an initial impression of the results (Fig. 4). The main limitations of this method, however, arise from the implicit assumptions that (a) the deformation occurs under plane strain conditions, and (b) the fault planes are the planes of the maximum shear stress.

The right dihedra method is based on the principle that the shear zone and the auxiliary plane (containing the normal to the shear zone and a line within the shear zone at 90° from the slip lineation) constitute a right dihedron dividing the stereogram in two opposite pairs of quadrants, one defining the field containing the σ_1-axis, the other delimiting the field for the σ_3-axis (McKenzie 1969, Angelier & Mechler 1977). This method examines each three-dimensional direction in turn and assigns a value to it denoting its suitability as a potential σ_1-axis. The suitability is defined by determining the proportion of the sample of faults for which the direction in question lies in the σ_1-quadrant. The numerical values associated with each direction are contoured. On the stereographic output, this orientation is represented as a field enclosed by the contour maximum. Conversely, the contours of minimum values enclose the position of σ_3-axis for most of the shear zones (Figs. 5e–h and 6e–h).

If the movement plane (the plane parallel to the fault's normal and its movement vector) is added to the right dihedron the resulting set of three mutually perpendicular planes form a right trihedron. The right trihedra method further narrows down the fields for the maximum and minimum stress axes. This is achieved by applying an additional condition, namely that the σ_1- and σ_3-axes must also lie in opposite pair of quadrants defined by the intersection of the auxiliary plane and the movement plane. With these boundary conditions, the program for the right trihedra method ('ROMSA' in Lisle 1988) calculates the likelihood for each possible orientation being parallel to the maximum principal stress (σ_1-axis). The points giving maximum likelihood are revealed by a contoured stereogram. The contour maxima indicates the directions that are common to the σ_1-trihedra for the maximum number of shear zones (Figs. 5i–l and 6i–l). In contrast to the right dihedra method, in the right trihedra method the lowest values obtained during the search of σ_1-axis do not automatically and necessarily signify the orientation of σ_3-axis. For this reason, a separate search for σ_3-axis is made in the right trihedra method (Figs. 5m–p and 6m–p).

Numerical methods developed and refined by Angelier (1984, 1990) lead to the determination of the reduced stress tensor defined by the orientations of the three principal stress axes and the shape of stress ellipsoid (Φ). We have used the 'direct inversion' and the 'four-dimensional exploration' methods of Angelier (1984, 1990). The underlying principle in both the methods involves minimization of the angle between slip lineation measured in the field and the direction of maximum shear stress calculated theoretically for every given shear zone of known orientation and sense of movement. The merits of 'direct inversion' over 'four-dimensional exploration' method are discussed in detail by Angelier (1990).

The numerical methods also yield two important measures of data dispersion *viz.* the 'ANG' and the 'RUP' indices (Angelier 1990). The parameter ANG defines the average angle between the slip lineation and the direction of the maximum shear stress computed from the estimated stress tensor. Although the value of ANG can range from 0° to 180°, in general, the results with average ANG of less than 45° are considered to be satisfactory (Angelier 1990). The second measure, RUP, is a function of the parameter ANG and the relative level of resolved shear stress magnitude. The value of RUP can vary between 0% and 200% corresponding to the ANG values from 0° to 180°, respectively. A critical analysis by Angelier (1990) reveals that the satisfactory palaeostress results from faults generally have a RUP value <50%.

The number of shear zones compatible with the computed stress tensor is given by P_{total}% in the right trihedra method of Lisle (1988). In the numerical methods, the percentage of shear zones with acceptable ANG and RUP values is denoted by a parameter called COH (Angelier 1984). Both P_{total}% and COH% indicate the goodness of results and are directly correlatable with each other.

The relative magnitude of stresses is expressed by the shape parameters **R** in the trihedra method and Φ in the direct inversion method (Lisle 1989a, Angelier 1990).

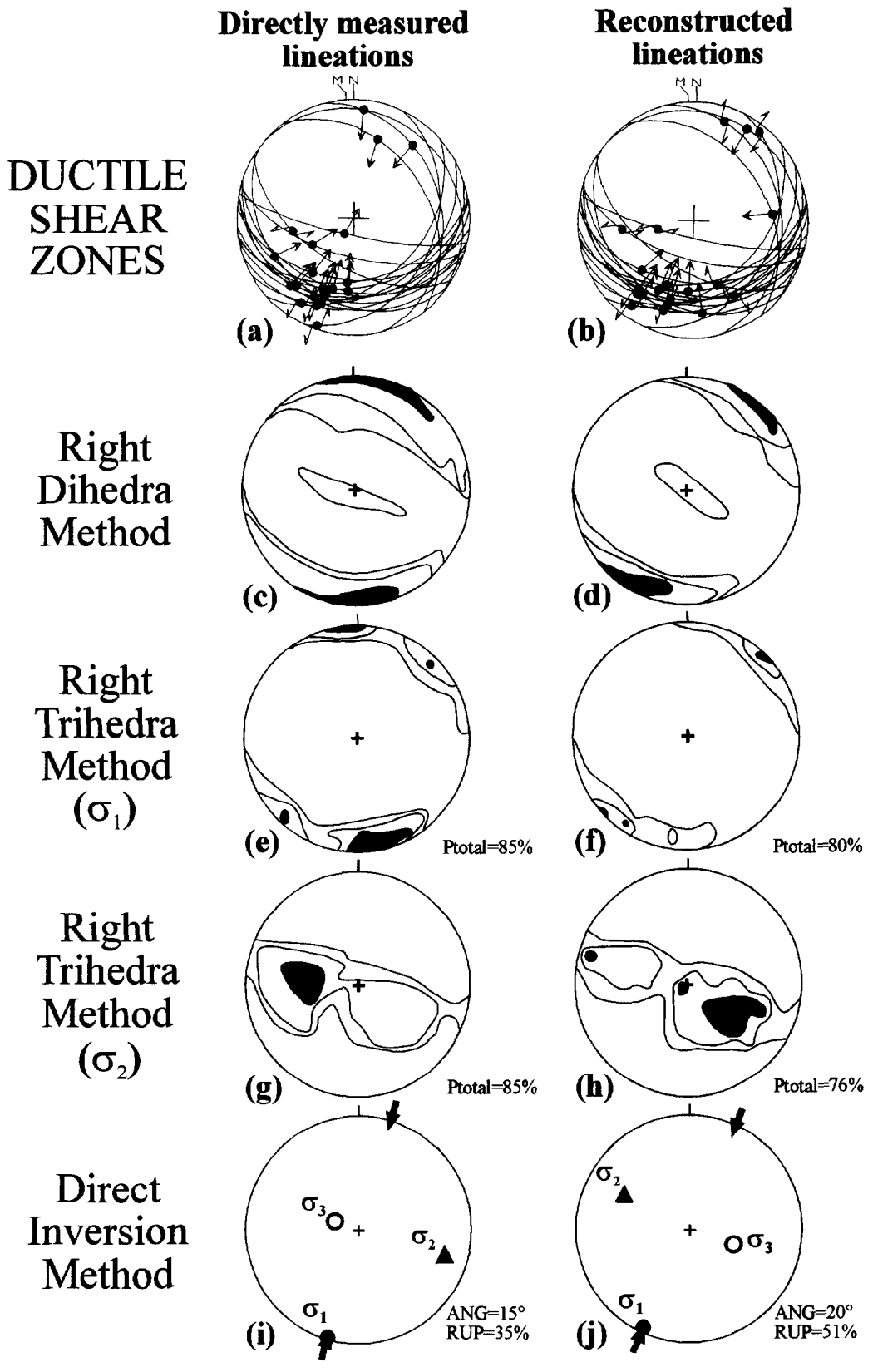

Fig. 9. Comparison of the results of palaeostress analysis of 22 ductile shear zones from the Tutt Head and Rams Tor sites. (a) Ductile shear zones with directly measured slip lineations. (b) Ductile shear zones with slip directions reconstructed by finding normal to the *S/C* intersection. (c) & (d) Results from the dihedra method (contour% 5–70–80–90 and 5–80–90–99, respectively). (e) & (f) Results from the trihedra method showing the most likely orientations of σ_1- axes. Contour % 60–70–80 in both the diagrams. (g) & (h) Results from the trihedra method showing the most likely orientations of σ_3- axes. Contour % 50–60–80 and 50–60–70, respectively. (i) & (j) Results from the direct inversion method (arrows indicate the direction of the maximum compression). P_{total}, ANG and RUP are explained in text. All lower hemisphere, equal area projections.

Both these parameters represent the ratio of differential stresses [$\mathbf{R} = (\sigma_2-\sigma_3)/(\sigma_1-\sigma_2)$ and $\Phi = (\sigma_2-\sigma_3)/(\sigma_1-\sigma_3)$] and are related by an expression $\Phi = \mathbf{R}/(1 + \mathbf{R})$. An advantage of **R** over Φ is the fact that the former can be represented on a Flinn diagram which can be conveniently divided into constrictional ($\infty > \mathbf{R} > 1$), plane ($\mathbf{R} = 1$) and flattening ($1 > \mathbf{R} > 0$) types of the stress states (Fig. 5 in Lisle 1989a). The abscissa and ordinate of such a Flinn diagram represent axially symmetric compression ($\mathbf{R} = 0$) and axially symmetric extension ($\mathbf{R} = \infty$), respectively.

RESULTS

The site-wise results of palaeostress analyses of the ductile- and brittle-ductile shear zones are summarized in Figs. 5 and 6 and Tables 1 and 2. For all sites, the same data are analysed by the *P–T* axes, the right dihedra, the right trihedra, the direct inversion (DIR INV) and the four-dimensional exploration methods. As both the direct inversion and four-dimensional exploration methods gave identical results, we present here only the results from the direct inversion method (Figs. 5q–t and 6q–t).

Only one representative diagram showing the results from the *P–T* axes method is given (Fig. 4). For each site, all the principal axes orientations obtained by the *P–T* axes method are further analysed by an orientation tensor procedure which takes into account the fact that the mean principal axial orientations must possess an orthogonal relationship (Lisle 1989b). The results of such statistical analysis of the *P–T* data are tabulated under the column of *P–T* axes in the Tables 1 and 2.

Development of the ductile shear zones in a thrust regime

The results of palaeostress analysis from the ductile shear zones reveal sub-horizontal orientations of the σ_1- and σ_2-axes at all the sites suggesting the development of these shear zones in a compressive and thrust tectonic regime (Figs. 5q–s). The σ_1-axis is oriented NNE on the southern limb (sites: Tutt Head and Rams Tor) and N–S to NNW on the northern limb (sites: Pier Head and Middle Head) of the Langland-Mumbles anticline. As the unfolding did not bring the orientations of the principal stresses on the two limbs any closer, the hypothesis that these shear zones were developed prior to the folding is not demonstrable. Despite the fact that the precise age of shearing with respect to folding remains unresolved, the difference in orientation of the shear zones on opposite limbs suggests that the orientation of mechanical inhomogeneity in form of bedding surfaces had a significant control on the orientation of the ductile shear zones.

In general, the values of **R** and Φ are very low ($< < 1$, Table 1) suggesting a relatively high σ_1 and approximately equal magnitudes of σ_2 and σ_3 during the ductile shearing. As a consequence of the axially symmetrical stress ellipsoid, orientation of the σ_2- and σ_3-axes were interchangeable. The instability in the orientations of σ_2 and σ_3-axes, revealed particularly well by the great circle girdle patterns in the results from the trihedra method (Figs. 5m–p), is possibly a consequence of the low values of the parameters **R** and Φ. The sub-vertical and sub-horizontal orientations of the σ_2- and σ_3-axes, respectively, shown by the direct inversion method at the Middle Head site are due to the combined effects of the symmetry of stress (low **R** value) and the scanty development of shear zones (Fig. 5t).

Development of the brittle-ductile shear zones in a strike-slip regime

The results from all the methods (except the dihedra method due to presence of several sub-maxima) reveal that brittle-ductile shear zones developed in a strike slip regime with sub-horizontal σ_1- and σ_3-axes directed towards NNE and ESE, respectively (Figs. 6i–t).

In contrast to the ductile shear zones, the brittle-ductile shear zones indicate remarkably consistent orientations of the principal axes on both limbs of the Langland-Mumbles anticline (Fig. 6 and Table 2). It is evident that the brittle mode of deformation was more dominant during this event as a result of which the en échelon fractures (veins) were developed regardless of the orientation of the local bedding planes. The brittle-ductile shear zones are distinctly post-folding structures and probably related to the regional-scale transverse faults with predominant strike-slip component in the area (Fig. 1b).

LIMITATIONS AND SOURCES OF ERROR

Our results show larger variability in comparison to the typical fault slip analysis results normally obtained by using brittle faults as the palaeostress indicators (Angelier 1990). These dispersions, reflected by the high values of the parameters ANG and RUP and the low values of P_{total}% (Tables 3 and 4), are indicative of the fact that a significant number of shear zones may not be compatible with the computed stress tensors.

One reason for large dispersion in the results could be that the shear zones produced under different stress conditions have been grouped together in one data set. In order to test this hypothesis, we subdivided the data of the ductile shear zones (from the Tutt Head site) into different subsets by rejecting the shear zones with larger values of the ANG ($> 45°$) in the three successive steps (Fig. 7). The data selected (with ANG $< 45°$) at the end of the first, second and third runs were analysed successively by the direct inversion method (subsets 1 to 3, Fig. 7).

With the progressive decrease of the sample size in the successive runs, significant improvements in the average

ANG and RUP values were achieved and eventually all the shear zones during the fourth run (COH = 100%) satisfied the conditions of acceptable ANG and RUP values (Fig. 7h). It is important to emphasize that in spite of these variations, neither the orientations of the principal stresses nor the symmetry of the stress ellipsoid (Φ) showed any significant change in the four sets of the results (Fig. 7). This consistency in the orientations of the principal axes and the shape of the stress ellipsoid (regardless of the sample size and the scatter in the result) along with the total lack of any geological evidence to suggest more than one generation of the ductile- or brittle-ductile-shear zones confirms that the large dispersion in our results is not due to the grouping of shear zones belonging to different stress tensors into a single data set.

The second possibility to account for the large dispersion may be the degree to which the assumption of the perpendicularity between the direction of maximum shear stress and the *S/C* intersection line is satisfied. In order to test the validity of this assumption, we have examined 22 shear zones (combined from Rams Tor and Tutt Head sites) that contain both calcite fibres parallel to the slip direction as well as *S/C* fabrics. For the same orientation of shear zones, two sets of data are generated, one with the directly measured slip lineations and the other with the slip directions reconstructed by determining a line perpendicular to the *S/C* intersection on the shear zone surface. For most of the shear zones the orientations of the directly measured and the reconstructed directions are close to each other (Fig. 8). In exceptional cases, however, the angular difference between the reconstructed directions of maximum shear stress and the directly measured lineations can be as much as 55°.

Both the sets of data have been analysed by the *P–T* axes, the right-dihedra and -trihedra and the numerical methods (Fig. 9 and Table 5). A critical comparison of the results reveals broadly consistent patterns in all the diagrams (Fig. 9). One of the main effects of reconstructing the slip lineations is the lowering of **R** and Φ values (Table 5). As a consequence of this, the σ_2- and σ_3-axes are somewhat differently oriented in the results from the direct inversion method (Figs. 9i–j and Table 5).

The other major effect of reconstructing the slip directions is reflected on the measures of the data dispersion (Fig. 9). In general, the values of RUP in the direct inversion method and ANG in the four-dimensional exploration method tend to be higher in the case of reconstructed shear directions. Similarly, a lower percentage of total faults (P_{total}%) is compatible with results from the right trihedra method during the search of both the σ_1- and σ_3-axes.

On the basis of these results we suggest that the higher RUP, ANG and lower P_{total}% in our analysis (Fig. 9) are largely a consequence of reconstructing the slip directions and the fact that these slip directions are at significant angular departure from the directly measured slip lineations, at least, in a few cases (Fig. 8). A greater degree of the homogeneity in the results from the brittle-ductile shear zones at Middle Head site (last row in the Table 4) is mainly due to the fact that the data available on this site are not sufficient in number to reflect the true heterogeneity of the sample.

DISCUSSION

Our results of an earlier thrust and later strike-slip event as well as the orientations of the principal axes during these two events are similar to those found by Roberts (1979) by an extensive study of tectonic joints in this area. Both the similarity in the pattern of stereographic results from different sites (Figs. 5 and 6) and the consistency of stress axes orientations obtained by different methods at individual sites further corroborate the validity of the results. These results are also consistent with an early thrust and late strike-slip motions in other fold and thrust belts (e.g. in the Appalachian Valley and Ridge, see Srivastava & Engelder 1990).

The palaeostress analysis of shear zones in the Langland-Mumbles area reveals a significant variation in the style of deformation (faulting) with the change in state of stress. At a time when the vertical stress (σ_v) corresponded to the minimum principal stress (σ_3), and thus when the mean stress was relatively high, the deformation was ductile type leading to the formation of abundant meso-scale ductile shear zones. With the lowering of the mean stress, implicit from the change of (σ_v) to become (σ_2), the ductile behaviour gave way to brittle deformation characterized by abundant Beach type-I en échelon veining in the area.

In spite of a larger scatter, our results demonstrate that the fault slip methods are applicable to the shear zones for the purpose of palaeostress analysis. As discussed earlier, the reason for larger scatter is the fact that in some shear zones the direction of maximum shear stress has a significant angular departure from the inferred slip directions.

If the veins within either set of conjugate shear zone represent extension fractures (mode-I), two different orientations of σ_3-axes, each perpendicular to veins in the set, are indicated by a given conjugate pair. Clearly, the Beach type-I vein systems are indicative of heterogeneous stresses on the scale of shear zones themselves and would seem to represent an obstacle for the application of our stress analysis. The results of palaeostress analysis, however, combine numerous data from both the sets and represent an integrated stress tensor on the scale of whole area or site and not on the scale of individual shear zones.

At least, in the study area, there is no geological evidence to suggest more than one phase of brittle-ductile- or ductile-shearing. In such cases, we recommend that the data must not be subdivided into different subsets in order to just reduce dispersion in the results. Geological evidence for sorting data into different subsets is most critical and must be sought.

CONCLUSIONS

Both ductile shear zones and brittle-ductile shear zones are suitable for palaeostress analysis by the fault slip methods. In areas where the slip lineations can be measured directly on the shear zone surface, the degree of homogeneity in results can be expected to be comparable to those obtained from the brittle faults. Reconstructing the slip directions contributes to a greater scatter in the results and in all such cases the assumption of slip lineation being normal to the *S/C* intersection must be tested by as many direct measurements as possible.

Despite limitations, the shear zones serve as useful palaeostress indicator as these structures reveal an unambiguous sense of the movement. In the absence of compelling geological evidence, the classification of data into different subsets with an objective of improving the homogeneity in the results can be insignificant geologically.

Acknowledgements—We are grateful to Professor J. Angelier for permission to use his program 'TENSOR' and to Dr Norman Fry for fruitful discussions. Thoughtful reviews by Professor Terry Engelder, Professor C. W. Passchier and Dr R. C. M. W. Franssen improved the paper greatly. This work was funded by the 'Marie Curie award' of the European Communities to DCS.

REFERENCES

Aleksandrowski, P. 1985. Graphical determination of principal stress directions for slickenside lineation population: An attempt to modify Arthaud's method. *J. Struct. Geol.* **7**, 73–82.

Angelier, J. 1984. Tectonic analysis of fault slip data sets. *J. geophys. Res.* **89**, 5835–5848.

Angelier, J. 1990. Inversion of field data in fault tectonics to obtain the regional stress—III. A new rapid direct inversion method by analytical means. *Int. J. Geophys.* **106**, 363–376.

Angelier, J. & Mechler, P. 1977. Sur une méthode graphique de recherche des contraintes principales également utilisable en tectonique et en séismologie: la méthode des dièdres droites. *Bull. geol. Soc. Fr.* **19**, 1309–1318.

Beach, A. 1975. The geometry of en échelon vein arrays. *Tectonophysics* **28**, 245–263.

Bénard, F., Mascle, A., Le Gall, B., Doligez, B. & Rossi, T. 1990. Palaeostress fields in the Variscan foreland during Carboniferous, microstructural analysis in the British Isles. *Tectonophysics* **177**, 1–13.

Bergerat, F. 1987. Stress fields in the platform at the time of Africa–Eurasia collision. *Tectonics* **6**, 99–132.

Berthé, D., Choukroune, P. & Jegouzo, P. 1979. Orthogneiss, mylonite and noncoaxial deformation of granites: the example of the South Armorican shear zone. *J. Struct. Geol.* **1**, 31–42.

Engelder, T. & Geiser, P. 1980. On the use of regional joint sets as trajectories of palaeostress fields during the development of the Appalachian plateau. *J. geophys. Res.* **85**, 6319–6341.

Etchecopar, A., Vasseur, G. & Daigenières, M. 1981. An inverse problem of microtectonics for the determination of stress tensors from fault striation analysis. *J. Struct. Geol.* **3**, 51–56.

Gephart, J. W. & Forsyth, D. W. 1984. An improved method for determining the regional stress tensor using earthquake focal mechanism data: an application to the San Fernando earthquake sequence. *J. geophys. Res.* **89**, 9305–9320.

Geological Survey of Great Britain 1971. Ordnance survey sheet SS-68-NW on 1: 10, 560 or 6 inches to 1 mile scale.

George, T. N. 1940. The structure of Gower. *Q. J. geol. Soc. Lond.* **96**, 131–198.

Hancock, P. L. 1985. Brittle microtectonics; principles and practice. *J. Struct. Geol.* **7**, 437–457.

Hyett, A. J. 1990. Deformation around a thrust tip in Carboniferous Limestone at Tutt Head near Swansea, South Wales. *J. Struct. Geol.* **12**, 47–58.

Letouzey, J. 1986. Cenozoic palaeostress pattern in the Alpine foreland and the structural interpretation in a platform basin. *Tectonophysics* **132**, 215–231.

Lisle, R. J. 1987. Principal stress orientation from faults: an additional constraint. *Annls Tectonicae* **1**, 155–158.

Lisle, R. J. 1988. ROMSA: a basic program for palaeostress analysis using fault striation data. *Comput. and Geosci.* **14**, 255–259.

Lisle, R. J. 1989a. Palaeostress analysis from sheared dike sets. *Bull. geol. Soc. Am.* **101**, 968–972.

Lisle, R. J. 1989b. The statistical analysis of orthogonal orientation data. *J. Geol.* **97**, 360–364.

Lisle, R. J. 1992. New method of estimating regional stress orientations: an application to focal mechanism data of recent British earthquakes. *Int. J. Geophys.* **110**, 276–282.

Marrett, R. & Allmendinger, R. 1990. Kinematic analysis of the fault-slip data. *J. Struct. Geol.* **12**, 973–986.

McKenzie, D. P. 1969. The relation between fault plane solutions for earthquakes and the direction of principal stresses. *Bull. seism. Soc. Am.* **59**, 591–601.

Michael, A. 1984. Determination of stress from slip data: fault and folds. *J. geophys. Res.* **89**, 11,517–11,526.

Pegaroro, O. 1972. Application de la microtectonique à une étude de neotectonique. Le Golfe Maliaque (Grèce centrale). Thesis, University of Montpellier.

Ramsay, J. G. & Allison, I. 1979. Structural analysis of shear zones in an Alpinized Hercynian granite, Maggia Nappe, Penine zone, Central Alps. *Schweiz. miner. petrogr. Mitt.* **59**, 251–279.

Ramsay, J. G. & Huber, M. I. 1983. *The Techniques of Modern Structural Geology (volume 1: Strain Analysis)*. Academic Press, London.

Roberts, J. C. 1979. Jointing and minor structures of the South Gower, peninsula between Mumbles Head and Rhossilli Bay, South Wales. *Geol. J.* **14**, 1–14.

Simpson, C. & Schmid, S. 1983. An evaluation of criteria to deduce the sense of movement in sheared rocks. *Bull. geol. Soc. Am.* **94**, 1281–1288.

Srivastava, D. C. & Engelder, T. 1990. Crack propagation sequence and pore-fluid evolution during fault-bend folding in the Appalachian Valley and Ridge, central Pennsylvania. *Bull. geol. Soc. Am.* **102**, 116–128.

Stauder, W. 1962. The focal mechanism of earthquakes. In: *Advances in Geophysics* (edited by Landsberg, H. E. & van Mieghem, J.). **9**, 1–71. Academic Press, London.

Tobisch, O. T., Fiske, R. S., Sacks, S. & Taniguchi, D. 1977. Strain in metamorphosed volcaniclastic rocks and its bearing on the evolution of orogenic belts. *Bull. geol. Soc. Am.* **88**, 23–40.

Turner, F. J. 1953. Nature of dynamic interpretation of deformation lamellae in calcite of three marbles. *Am. J. Sci.* **251**, 276–298.